Effective connectivity in cortical networks during deception: a lie detection study using EEG

Effective connectivity in cortical networks during deception: A lie detection study using EEG

Junfeng Gao, Xiangde Min, Hua Zheng, Anne Manyande, Huifang Si, Xuebi Tian,

Huimiao Zhan, Qiannuo Kang, Yinhong Dong, Chenhong Li, Pan Lin, Jian Song

***Abstract*—Previous studies have identified activated regions associated with deceptive tasks and most of them utilized time, frequency, or temporal features to determine deceptive responses. However, when deception behaviors occur, the functional connectivity pattern and the communication between different brain areas remain largely unclear. In this study, we explored the most important information flows between different brain cortices during deception. First, we employed the guilty knowledge test protocol and recorded on 64 electrodes' electroencephalogram (EEG) signals from 30 subjects (15 guilty and 15 innocent). EEG source estimation was then performed to compute the cortical activities on the 24 regions of interest (ROIs). Next, effective connectivity was calculated by partial directed coherence (PDC) analysis applied to the cortical signals. Furthermore, based on the graph theoretical analysis, the network parameters with significant differences were extracted as features to identify two groups of subjects. In addition, the ROIs frequently involved in the above network parameters were selected and based on the difference in the group mean of PDC values of all the edges connected with the selected ROIs, we presented the strongest information flows (MIIF) in the guilty group relative to the innocent group. Experimental results first show that the optimal classification features are mainly in-degree and out-degree measures of the ROI and the high classification accuracy for four bands demonstrated that the proposed method is suitable for lie detection. In addition, the frontal-parietal network was found to be most prominent among all the MIIFs in four bands. Finally, combining the neurophysiology signification of four frequency bands, respectively, we analyzed the roles of all the important information flows to uncover the underlying cognitive processes and mechanisms used in deception.**

***Index Terms* — effective connectivity, partial directed coherence, cortical network, lie detection**

Ⅰ. Introduction

Lying is an inevitable fact of our daily life. It is well known that deception is intrinsically a high-level cognitive event which involves complex cognitive functions such as executive control and working memory representation [1]. Hence, lie detection (LD) using neuroimaging (e.g., fMRI) or neurophysiological signals (e.g., ERP), has drawn much attention in the past 2 decades [2], [3]. Recently, accumulated evidence has consistently revealed the high efficiency of ERP-based LD methods [4]. In addition, a number of methods using the ERP have been proposed and successfully used in LD [5], [6].

For EEG-based LD, one of the important tasks is to extract ERP features to differentiate deceptive from truthful responses to the stimuli. Most previous methods, such as the bootstrapped correlation difference and the bootstrapped amplitude difference, only focused on the information extracted from single or several scalp sensors. For example, three scalp sites including Fz, Cz and Pz were frequently utilized in LD [4]-[7]. Furthermore, in our early reports [8]-[11], various ERP features at several sites were extracted to identify lying behavior. Similarly, most fMRI-based studies only explored the brain-activity pattern (or activated brain regions) during processing deceptive tasks [1]-[3].

Cognitive functions are likely to be implemented by coordinating interactions of neural assemblies distributed in the brain [12]. Extensive evidence indicates that understanding brain function not only requires collecting information separately from involved brain areas but also requires exploring functional interactions across different brain regions [13]. Lying is a complex cognitive process involving multi brain cortices, which have been demonstrated especially by many fMRI-based LD studies [2], [3], [13], [14]. Over the past several decades, in spite of extensive EEG-based LD research, few studies recording multi-channel EEG signals employed

Junfeng Gao, Huimiao Zhan, Qiannuo Kang, Yinhong Dong and Chenhong Li are with the Key Laboratory of Cognitive Science of State Ethnic Affairs Commission, College of Biomedical Engineering, South-Central University for Nationalities, Wuhan 430074, China (junfengmst@163.com; zhanhm6@163.com; Kang_980214@163.com; dyh4@163.com; lichen@mail.scuec.edu.cn).

Xiangde Min is with the Department of Radiology, Tongji Hospital, Tongji Medical College, Huazhong University of Science and Technology, Wuhan, 430030, China; the first three authors contributed equally to this work.

Hua Zheng and Xuebi Tian are with the Department of anesthesiology, Tongji Hospital, Tongji Medical College, Huazhong University of Science and Technology, Wuhan 430030, China (email: hzheng@hust.edu.cn; tianxb@hust.edu.cn).

Anne Manyande is with the School of Human and Social Sciences, University of West London, London W5 5RF, United Kingdom (email: Anne.Manyande2@uwl.ac.uk)

Huifang Si is with the Zhuhai Maternity and Child health hospital (Zhuhai Women's and Children's Hospital), Zhuhai, 519000, China (email: lemon7_up@163.com).

Pan Lin is with the School of Education Science, Hunan Normal university. Changsha, Hunan, China (tiger.lin9906@gmail.com).

Jian Song is with the Department of Neurosurgery, General Hospital of the Central Command Theater of PLA, Wuhan, 430070, China (e-mail: docsongjian@yahoo.com).

Corresponding authors: Pan Lin and Jian Song.

brain connectivity or network methods to detect lying [15]-[17]. In fact, networks of the brain nervous system have been widely used as a way to describe interactions between different cortical regions, and to understand the organized behavior of cortical regions [18], [19]. Hence, despite high identification accuracies frequently reported in existing investigations, the brain connectivity pattern and mechanisms underlying deception deserve further investigation.

There are currently two different types of brain connectivity: functional connectivity (FC) and effective connectivity (EC) [20]. Compared to the former, EC can provide more interaction information with not only strength but also directions between the two systems. To date, a number of specific measurements have been proposed to estimate EC, such as directed transfer function and Partial-Directed Coherence (PDC) [21], [22]. Moreover, some of them can only compute EC in the time domain, whereas others can search for frequency-specific interactions. Indeed, it has been acknowledged that information in the frequency domain is more important than that in the time domain for understanding EEG signals [23]. Hence, to deeply understand the neural processing underpinnings of deception, it is necessary to concurrently characterize both the spectral and directional properties of the brain connectivity, which to our best knowledge has never been conducted or reported in the studies related to deception.

Furthermore, most current studies have performed scalp level brain connectivity analysis. Due to the influence of volume conduction on the EEG [24], each EEG channel measures a mixture of signals coming from different cortex locations. As a result, measuring connectivity between these scalp channels mostly picks up spurious connections. Apart from the above limitation, scalp EEG has poor ability to localize brain function results to different cortex regions due to low spatial resolution. Hence, evaluating neural activities, using brain connectivity measured from scalp EEG is unsuitable and would increase the problem of interpreting the neural mechanism of lying. To our knowledge, few studies of cortical FC and networks have been conducted on EEG-based LD [17], and more importantly, no study has yet been devoted to the cortical EC during deception processing.

Abovementioned limitations in current EEG-based LD research prevent a deep understanding of the brain function mechanism during deception. In this study, in order to fill in the theoretical gap in current LD studies, we aimed i) to explore the difference in effective brain connectivity and networks on the cerebral cortex between deceptive and truthful behaviors, and then to uncover the neurophysiological mechanisms of deceptive behaviors and ii) to set up an effective machine-learning classification system that could distinguish truth-telling from lie-telling based on the features extracted from the abovementioned brain networks. For the above purposes, first, the cortical current density on the 24 regions of interest (ROI) was estimated by employing the linear inverse procedure [25] on the scalp EEG from two groups of subjects. Following that estimation, by applying the partial directed coherence (PDC) measurement to cortical waveforms, we explored the EC patterns on these ROIs in each frequency band of interest. Furthermore, using a graph theoretical approach, we characterized topographical properties of the above resulting networks, and based on the statistical analysis we selected those parameters with significant differences between the guilty and the innocent groups, which were used to construct feature vectors and then fed into a support vector machine (SVM) [9] to implement the identification task. More importantly, we finally constructed and analyzed the most important EC between the key ROIs based on the above resulting network parameters to explore the brain neural mechanism underlying deception behaviors.

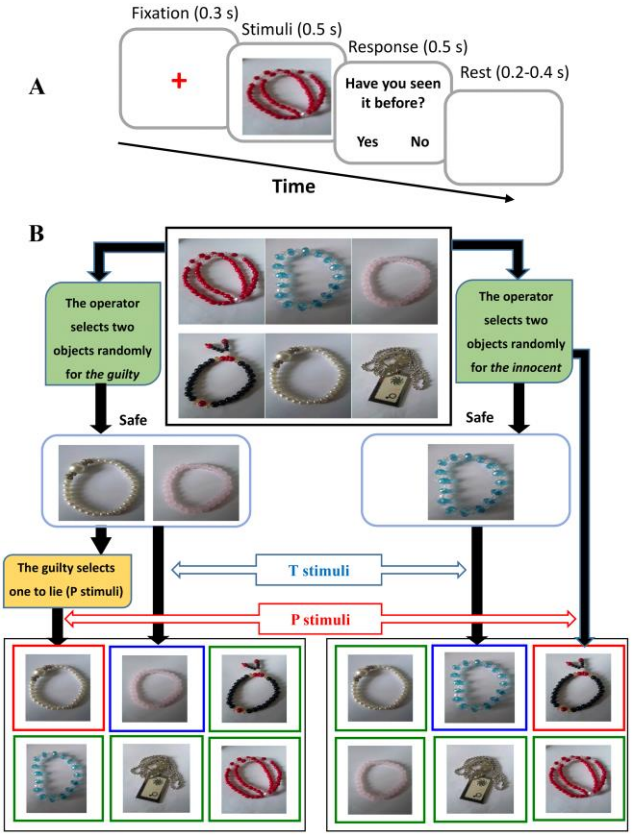

Fig.1. Protocol of the stimuli and the experimental design (A) the time sequence of the four stages within a trial: fixation stage (0.3 s), stimuli presentation stage (0.5 s), responding stage (0.5 s) and resting stages (0.2-0.4 s). (B) the experimental design for the guilty and innocent groups, respectively.

II. METHOD

A. Subjects and Ethics statement

After participants were given a detailed explanation of the experimental procedure, they wrote down their informed consent. The study was approved by the Psychology Research Ethical Committee in South-Central University for Nationalities. Thirty healthy right-handed undergraduate students were recruited and then randomly divided into guilty (7 females, mean age: 21.2 ± 1.2) and innocent groups (7 females, 21.3 ± 1.5). It was confirmed that all participants had no history of psychiatric or neurological illness by a prior psychiatric clinical assessment.

B. Procedure and tasks

The guilty knowledge test (GKT) [4] was employed, which

is a type of oddball paradigm and can test a suspect's memory about a crime. Six different jewels and their pictures were prepared. For the guilty subjects, we gave them two jewels in a box and instructed them to steal one and memorize its characteristics carefully, which was the probe (P) stimulus, while the other one in the box was the target (T) stimulus. For the innocent subjects, they only saw one jewel in the box and stole nothing, which was the T stimulus. The P stimulus was selected randomly from the remaining five objects. For two groups, the remaining four pictures were Innocent (I) stimuli. The other details can be found in our earlier study [15].

During the experiment, all participants were asked to try to fixate their gaze on the center of the screen in order to avoid serious EMG or EOG artifacts. Each trial started with a fixation stage (0.3 s) and a cross-fixation in the center of the screen. Subsequently, the stimulus lasting for 0.5 s was presented, which was immediately followed by a question ("Have you seen it before?") on the center of the screen to promote a response within 0.5 s. Responses were presented using a button box in their hand with two keys (the left button for "Yes" means that the subject has seen the stimuli before the recording stage, whereas the right one for "No" means that he/she has not seen the stimuli before). During the responding stage, the guilty subjects replied deceptively and pressed "No" button when they were faced with the P stimuli. However, they responded honestly to the T and I stimulus. In contrast, the innocent subjects honestly responded to three types of the stimuli. The presentation of each stimulus was edited and controlled by the E-prime software (version 3.0) according to a pseudo-random sequence.

Finally, each trial ended with a resting stage lasting between 0.2 and 0.4 s (0.3 s, on average) with a blank screen (see Fig. 1A). The varied ISI (inter-stimulus interval) was set to avoid emotional effects caused by the procedure of the previous trial. There were 180 stimuli in total, including 30 T (16.7% of all stimuli), 30 P (16.7% of all stimuli) and 120 I stimuli (66.6% of all stimuli) in each session lasting about 5 minutes. Each subject repeated the above-mentioned session 4 times, and the resting interval was 3 minutes.

At the end of the experiment, each subject was given 100 RMB. To emphasize the social nature of the lying task, the guilty subjects were told before the task that their brain signals, eye movement and facial expression will be analyzed after the task to determine if they lied. If they successfully concealed the identity of the task, they received an additional bonus of 50 RMB.

C. EEG recording

We recorded EEG on 64 standard scalp electrodes and referred to bilateral mastoids using a NeuroScan amplifier (Charlotte, NC, USA). Electrode impedances were below 5 $K\Omega$. The A/D sampling rate was 500Hz and the bandwidth of amplifiers was 0.1-70 Hz. The vertical EOG signal was recorded from the right eye (2.5 cm below and above the pupil), and the horizontal EOG signal was recorded. Using the auto-regressive model in the NeuroScan system, we first rejected eye movement from the EEG. Second, visual inspection of the EEG was performed and the segments with serious saccades and EMG artifacts were excluded. Trials with

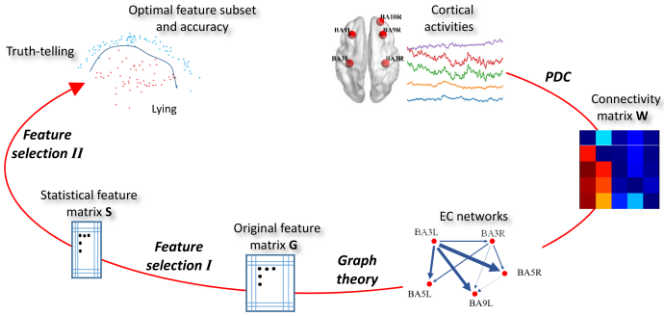

Fig. 2. Schematic illustration of the pipeline of the proposed method. Feature selection I was implemented by applying statistical analysis on the original 81 graph-based features separately. The number of columns in matrix **S** is less than that in matrix **G** based on the statistical comparison between the two groups. Feature selection II was implemented by combining the F-score with SVM classification. Five BAs in the figure are used to exemplify only.

incorrect responses were eliminated from the EEG data, and any epochs that had a voltage exceeding $\pm 75\ \mu v$ were excluded.

Using the EEGLAB toolbox [26], each continuous EEG signal was first cut into epochs from -300 to 1200 ms after stimuli presentation. Second, based on the pre-stimuli interval, all of the epochs were baseline-corrected. Following the correction, an independent neurophysiological expert checked the grand average on each electrode for each subject. If no P300 was found simultaneously on Fz, Pz and Oz sites in the T responses, the subject's experimental data were excluded. The result is that no one was excluded. Third, only for the P responses within each subject, we averaged across sequential sets of 5 trials to enhance the signal-to-noise ratio of the EEG, resulting in 300 averaged P trials (25 trials × 4 sessions × 15 subjects ÷ 5) for each group of subjects. Finally, from each resulting trial, we retained the trial from 0.1 s to 0.7 s after stimuli representations, cutting the other time stages, to conduct the subsequent analysis.

D. ROIs selection and cortical activity estimation

We selected 24 ROIs out of 84 Brodmann areas (BAs) and listed them in Table I, which are consistently found in most current LD investigations using EEG or fMRI. Following the definition of ROIs, the cortical activities were estimated by the application of the linear inverse procedure [25] from scalp EEG signals to the source space.

In this study, the sLORETA source estimation [27] was employed, yielding the cortical activities on the 24 ROIs from each trial. sLORETA is based on the smoothest solution of the inverse problem as the most plausible one. The solution space is restricted to the cortical gray matter in the digitized Montreal Neurological Institute (MNI) atlas with a total of 6239 voxels at 5 mm spatial resolution. Using sLORETA, the voxel at the centroid of each BA was used to calculate the current density and hence the results represent the activity of the corresponding BA, in which a standard head model of the boundary element model in the software was used.
The complete analysis procedure is illustrated in Fig. 2, taking 5 ROIs as an example.

E. Principle of PDC and EC estimation

PDC has been widely used in EC analysis[28], which represents direct causal influences of one region on another

[29]. In this study, PDC was selected to characterize EC in the cortical space for four principal frequency bands.

Using the above PDC algorithm, the asymmetric weighted connection matrix $\mathbf{W}$ was obtained in each frequency band for each trial in the cortical space, in which each matrix coefficient $\mathbf{W}_{ij}$ corresponded to the PDC value from the ROI j to the other ROI i. When $i = j$, the coefficient in the matrix was set as 0. Based on these connection matrices, we calculated and obtained 1200 EC networks (300 trials $\times$ 4 bands) for each group of subjects, each of which involved 24 nodes corresponding to the ROIs and 24×23 edges.

F. Graph analysis for feature extraction

Graph theory is frequently applied to analyze the structure and evolution of complex networks, which provides a powerful mathematical framework for characterizing its topological properties [29], [30]. We extracted 4 local measures to characterize the features of each node, including in-degree D_{in}, out-degree D_{out}, clustering coefficient C and local efficiency E_{loc}. Also, 4 global measures were extracted to characterize the overall property of the network, including averaged clustering coefficient C_A, characteristic path length L_W, global efficiency E_{glob} and small world index γ [31]. For the index γ, the BCT toolbox [32] was used to generate 50 surrogate random networks which were derived from the original networks by randomly reshuffling the edge weights in the network [30].

The result of the above graph analysis was stored as a 600 $\times$ 100 matrix (600 networks for two groups) in each frequency band, and the dimension of the original feature vector was 100 (24 nodes $\times$ 4 local features + 4 global features), which is hereafter called the original feature matrix **G** (see Fig. 2) and further processed by feature selection.

G. Feature selection I based on statistical methods

There were two steps of feature selection in order to remove redundant features. The first step, referred to as feature selection I, was conducted by statistics. Statistically significant differences were assessed for each feature separately in each frequency band using the independent samples *t-test* with the subject type as the grouping variable (df = 598). Considering that the number of local features were remarkably more than that of the global features, we performed the statistical test separately over the global and local features. The Bonferroni correction was employed to account for multiple comparisons. Thus, for the statistics of local and global features, the alpha-level was $p < 0.01/96$ (96 local features) and $p < 0.01/4$ (4 global features), respectively. From the above statistical analysis, those features without significant differences between the two groups were removed from the original feature matrix **G**, resulting in a new matrix for each band, referred to as the statistical feature matrix **S** (see Fig. 2), which was subsequently fed into the procedure of the feature selection II.

H. Feature selection II combined with classification

Table I. The locations of 24 selected ROIs from the segmented 84 Brodmann areas.

No.	Hemisphere	BA	Anatomical landmark	Lobe	MNI coordinates		
					x	y	Z
1	L	6	Middle Frontal Gyrus	Frontal Lobe	-30	-5	55
2	R	6	Middle Frontal Gyrus	Frontal Lobe	30	-5	55
3	L	7	Precuneus	Parietal Lobe	-20	-65	50
4	R	7	Precuneus	Parietal Lobe	15	-65	50
5	L	8	Superior Frontal Gyrus	Frontal Lobe	-20	30	50
6	R	8	Superior Frontal Gyrus	Frontal Lobe	20	25	50
7	L	9	Middle Frontal Gyrus	Frontal Lobe	-30	30	35
8	R	9	Middle Frontal Gyrus	Frontal Lobe	30	30	35
9	L	10	Frontopolar area	Frontal lobe	-25	55	5
10	R	10	Frontopolar area	Frontal lobe	25	55	5
11	L	13	Insular cortex	Occipital Lobe	-10	-90	0
12	R	13	Insular cortex	Occipital Lobe	10	-90	0
13	L	24	Dorsal anterior cingulate cortex	Limbic lobe	-5	-50	5
14	R	24	Dorsal anterior cingulate cortex	Limbic lobe	5	-50	5
15	L	32	Dorsal anterior cingulate cortex	Temporal Lobe	-45	-55	-15
16	R	32	Dorsal anterior cingulate cortex	Temporal Lobe	45	-55	-15
17	L	40	supramarginal gyrus	Frontal Lobe	-50	20	15
18	R	40	supramarginal gyrus	Frontal Lobe	50	20	15
19	L	44	Precentral Gyrus	Frontal Lobe	-50	10	15
20	R	44	Precentral Gyrus	Frontal Lobe	50	10	15
21	L	46	Middle Frontal Gyrus	Frontal Lobe	-45	35	20
22	R	46	Middle Frontal Gyrus	Frontal Lobe	45	35	20
23	L	47	Inferior prefrontal gyrus	Frontal Lobe	-30	25	-15
24	R	47	Inferior prefrontal gyrus	Frontal Lobe	30	25	-15

MNI：Montreal Neurological Institute; BA：Brodmann area; R：right; L：left.

The second step of feature selection is called feature selection II. We applied the wrapper strategy [33], [34] to select an optimal feature subset by combining with a classification procedure. Fig. 3 illustrates this strategy for each band. First, on the whole feature sample, a 15-fold subject-wise cross-validation (SWCV) [8], [35], [36] method was used. Specifically, in each fold of the SWCV, the samples of the 28 subjects (14 guilt and 14 innocent subjects) were used as training data $\mathbf{D}_{tra}$, whereas the samples from the remaining two subjects were used as testing set $\mathbf{D}_{tes}$ in order to assess the generalizability of the classification model. Subsequently, the F-score, a typical feature selection method, was performed on the training set $\mathbf{D}_{tra}$. The details of this method can be seen in our previous studies [9], [35] and other reasearches [37]. [38]. Following the SWCV, a 10-fold CV [3], [8], [11], [35] was applied on $\mathbf{D}_{tra}$ to overcome the overfitting problem. Hence, we constructed 10 pairs of subtraining set $\mathbf{D}_{stra}$ and validation set $\mathbf{D}_{val}$, in which $\mathbf{D}_{stra}$ was used to train the classifier and the set $\mathbf{D}_{val}$ to assess the trained classifier, respectively [8], [38] The evaluation measures for the classification system include:

a) Balanced Validation Accuracy (BVA): For each training set $\mathbf{D}_{tra}$, by using the 10-fold CV, *BVA* was the average of 10 pairs of sensitivities and specificities. In order to compare the *BVAs* with different feature subsets and classifier parameters, we obtained the optimal feature subset and classifier when the *BVA* reached the highest level. Note that the above optimal results might be different for different set $\mathbf{D}_{tra}$.

b) Balanced Testing Accuracy (BTA): Testing the above trained classifier using the set $\mathbf{D}_{tes}$ with selected optimal features as the feature vector, we obtained a *BTA* (an average of the sensitivity and specificity). Hence, by using the SWCV, we obtained the average of all the 15 *BTAs*, which is reported as *ABTA ± SD (mean ± standard deviation)* in this study. Due to the possible different results of optimal results when using different pairs of set $\mathbf{D}_{tra}$ and set $\mathbf{D}_{tes}$, we decided on the final optimal feature set and corresponding optimal classifier (and its parameters) when the *BTA* reached the highest level among all the 15 *BTAs*, which we reported.

For each training, we selected SVM (support vector machine) classifier [8] with a RBF, (radial basis kernel function) ($K(x,y)=e^{-\|x-y\|^2/g}$) as the classifier [39] and the radial width of the function g set from 2^{-5} to 2^5 with a step of 2; the regularization parameter was set from $C = 2^{-5}$ to 25 with a step of 2 during each training procedure.

I. Analysis of the most important information flow on ROI

We focused on measures that could reflect more complex workload in the specific brain regions during lying, relative to truth telling. Hence, among the above resulting optimal feature subset, we selected the measures whose value was significantly greater in the guilty group than in the innocent group, which hereafter is referred to as *focused measures*. Subsequently, for the ROI involved in each local focused measure, we calculated the difference in the group mean of PDC values of all the edges connected with the ROI. Finally, we sorted the above differences in descending order for each ROI, resulting in a maximum difference value for each ROI (i.e., the strongest information flow in the guilty group relative to the innocent group) which is hereafter referred to as *the most important information flow* (MIIF) for each ROI for each measure.

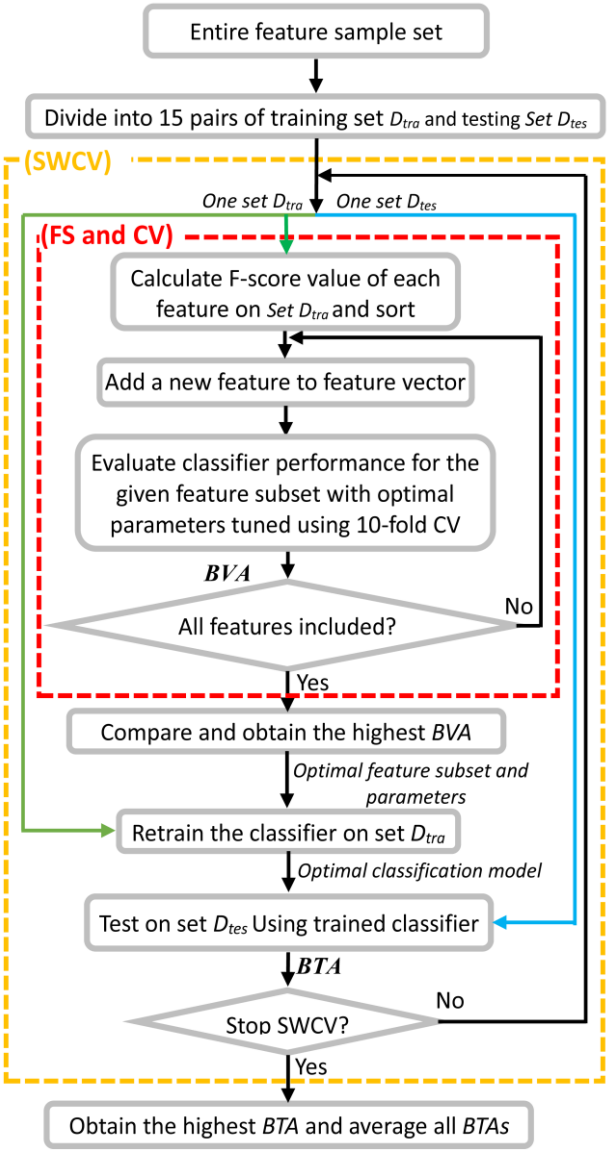

Fig. 3. Flow chart of the feature selection (FS) and classification. The dataset and computation results are expressed in italics. The green and blue lines represent the input of the training set and testing set, respectively. CV: cross validation. SWCV: subject-wise CV. *BVA*: balanced validation accuracy; *BTA*: balanced testing accuracy.

III. Results

A. EC matrix estimation

Using the PDC method on each cortical trial on the 24 ROIs, the weighted connectivity matrix $\mathbf{W}$ in each interested frequency band was obtained. The two group mean matrices in each band are shown in Figure 4. By visual inspection, obvious differences in PDC values between the two groups can be found on some pairs of ROIs in each band.

B. Feature selection I

Using the graph theory, a feature vector of 100 dimension was extracted from each EC network, resulting in the feature matrix **G**. Firstly, examination of the normality of distribution was performed on each feature. The result shows that the condition of normality of the distribution was not satisfied on most of the features. Hence statistical analysis was performed with nonparametric independent sample Wilcoxon rank-sum (Mann-Whitney) and the result reveals that there are 61, 64, 67 and 59 features with significant differences between the two groups in four bands, respectively. Hence, the statistical matrix **S** was obtained with 61, 64, 67 and 59 columns for the four bands, respectively.

C. Feature selection II and classification

The feature selection II combined with the classification was performed on the statistical matrix **S**. Fig. 5 presents the classification performance results as a function of the number of the sorted features. As observed in Fig. 5, the accuracy reached the maximum value when a few features were used for all four bands. In addition, we obtained the optimal feature

Table II. Classification accuracy (mean ± SD) for the four bands

Frequency bands	Classification accuracy				The number of the optimal feature subst
	Training		Testing		
	Sensitivity	Specificity	Sensitivity	Specificity	
Delta	99.67 ± 0.0012	97.41 ± 0.0060	97.00 ± 0.0532	96.05 ± 0.0699	17
Theta	99.59 ± 0.0056	97.52 ± 0.0058	98.67 ± 0.0281	98.33 ± 0.0527	8
Alpha	100.00 ± 0.000	99.63 ± 0.0035	98.52 ± 0.0322	99.00 ± 0.0316	16
Beta	99.56 ± 0.0023	99.70 ± 0.0016	98.44 ± 0.0422	99.67 ± 0.0105	20

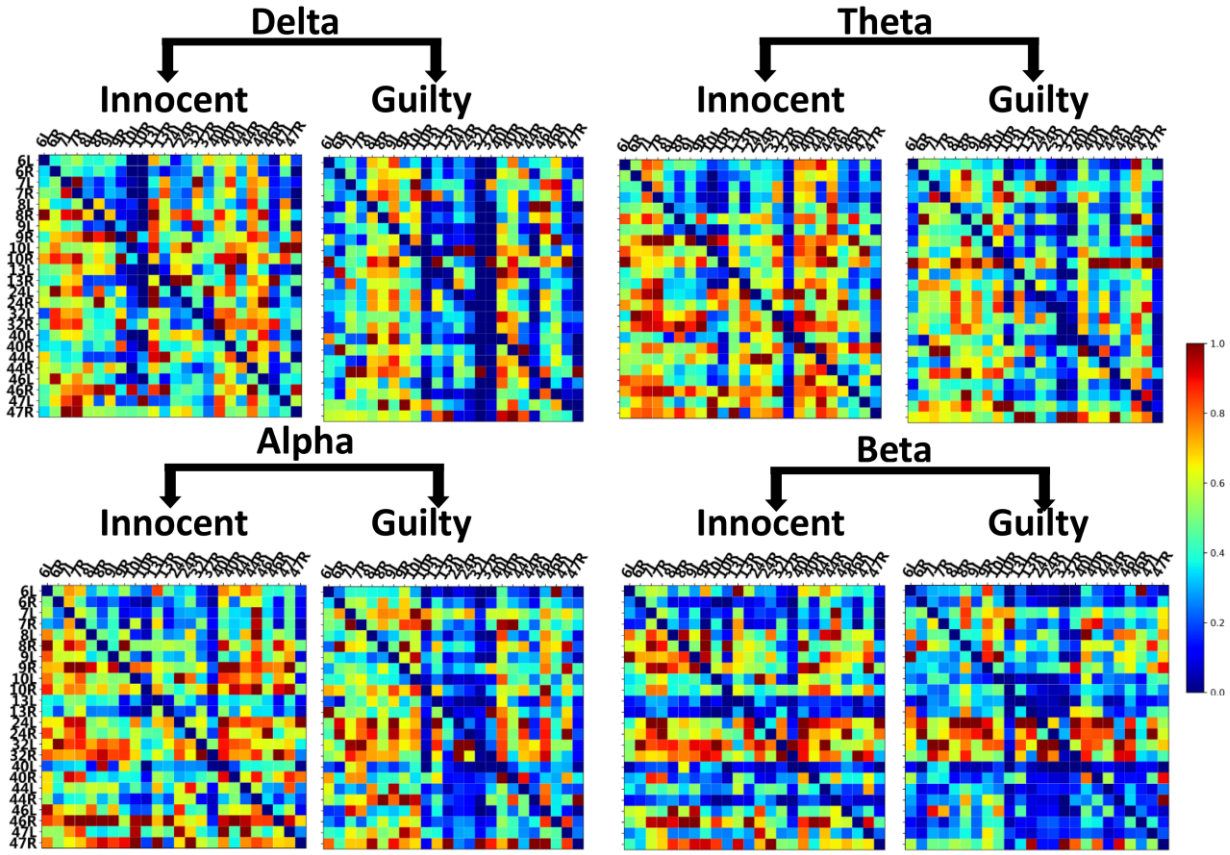

Fig. 4. Grand averaged PDC connectivity matrices of the innocent and guilty groups in four frequency bands. Each matrix is a 24*24 square matrix, where X axis and Y axis correspond with the ROIs, and each cell represents the mean strength of the PDC between specific pairs of regions. The strength of the PDC is indicated with a color scale, from blue (PDC = 0) to red (PDC = 1).

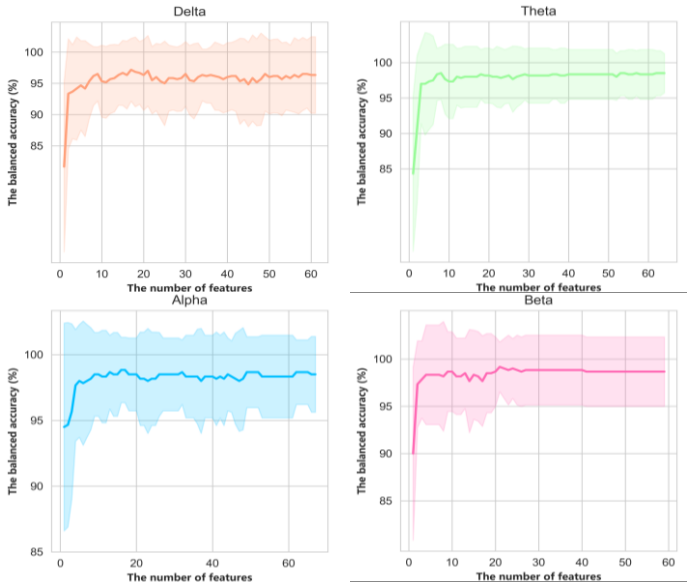

Fig. 5. Classification performance as the function of the number of the features for the four bands. Curve represents the *ABTA* and the ribbon of the curve denotes the SD of the *ABTA* using 15-fold SWCV.

subset based on the highest *BTA*. The result shows that there are 17, 8, 16 and 20 features constructing the optimal feature subset and the corresponding *BTA* are 96. 53%, 98.50%, 98.76% and 99.06% for the four bands respectively. Finally, the accuracy results are reported in Table II along with the number of the optimal feature subset for the four bands.

D. The most important information flow for ROI

The group means of the optimal features were compared and are shown in Fig. 6. First, it shows that most of the values of the guilty group are significantly lower than those in the innocent group for the four bands. Second, only one globe measure (*Lw*, in delta band) is included in the optimal feature subset for four bands. The focused measures were obtained and are listed in Table III. It shows that most of these measures are in and out degrees. Furthermore, the MIIFs for the ROIs in those focused measures were calculated and are reported in Table IV, along with the EC group mean on each MIIF. Specifically, for the local measure E_{loc}_32L, the input flow and out flows on BA 32L were analyzed separately using the proposed method. Interestingly, there are all negative differences in group mean on the output flow on BA 32L between the two groups (i.e., the EC value on each output flow from BA 32L in the guilty group is lower than that in the innocent group). Hence, we only selected the input MIIF on BA 32L to construct EC networks. The above results are summarized in Table IV.

Table III. The focused measures

Measures	Delta	Theta	Alpha	Beta
D_{out}_46R	●	●	●	●
D_{in}_44R	●	●	●	●
D_{in}_7LR			●	●
D_{out}_10R			●	●
D_{out}_10L				●
D_{in}_13R				●
E_{loc}_32L				●
L_W	●			

Symbol ● denotes the measure is in the band

Based on this result, the EC networks constructed by the MIIFs are illustrated in Fig. 7 for each band. Using the independent samples *t*-test separately on EC values of each MIIF as shown in Table IV, we found them all to have significant differences between the two groups ($p < 0.003$ with Bonferroni correction).

IV. Discussion

A. Cortical functional connectivity during deception

Current EEG-based lie detection methods are primarily based on few electrodes and employed in the time-frequency features of ERPs instead of the cortical current density. Furthermore, most fMRI-based studies only focused on activated brain cortices during a subject's engagement in a deceptive task. Throughout the past decade, although much knowledge has been acquired about activated brain regions or extracted features on the EEG using various deception tasks, little attention has been focused on brain functional cooperation in different brain regions during deception. We utilized PDC as a new lie detection method to characterize network patterns on the brain cortex. PDC was selected to characterize EC in the cortical space for four principal frequency bands. To our knowledge, no deception investigation has yet been conducted exploring the direct causal influences of one brain region on another region in different frequency bands. Furthermore, we assessed the MIIFs between different cortices in different bands to analyze the cognitive processes and brain activity mechanisms underlying deceptive tasks. The details about these MIIFs are as follows.

1) Frontal-parietal network and its contribution to the lying behaviors

The involvement of the frontal-parietal network in the behavior of lying has been repeatedly reported in a variety of lying studies. Fig. 7 shows that the communications within the cortices from the frontal-parietal network, including BA 7, BA 9, BA 10, BA 44, and BA 46, are the MIIFs on all four bands.

Within the frontal cortex, first, a large amount of the most recent evidence has consistently indicated that the involvement of the dorsolateral prefrontal cortex (DLPFC) is frequently involved in cognitive processes related to attention or the detection of motivationally salient stimuli [41]-[45]. In our protocol, the P stimuli are more highly salient for the guilty than that for the innocent. In a MEG study, Ishii et al. [46] also demonstrated that synchronization in the delta band is highly associated with the attention and memory updating processes. In this study, within the DLPFC, the MIIFs include the connectivity between BA 9R and BA 46R on the delta band, which might indicate stronger attention on P stimuli and more process load of the working memory for the guilty group, in contrast to the innocent group.

Table IV. MIIFs (most important information flows) and corresponding group mean on each band

Measures	MIIFs and group mean of PDC											
	Delta			Theta			Alpha			Beta		
	MIIF	Guilty	Innocent	MIIF	Guilty	Innocent	MIIF	Guilty	Innocent	MIIF	Guilty	Innocent
D_{out}_46R	46R→9R	0.2215	0.0004	46R→6L	0.2719	0.0140	46R→6L	0.4185	0.0514	46R→6L	0.4160	0.0526
D_{in}_44R	44R←7L	0.2377	0.0012	44R←46R	0.2075	0.0182	44R←10L	0.1468	0.0085	44R←10L	0.0757	0.0526
D_{in}_7L							7L←46R	0.2236	0.0201	7L←46R	0.1574	0.0099
D_{out}_10R D_{in}_7R							10R→7R	0.2453	0.0013	10R→7R	0.2053	0.0005
D_{out}_10L										10L→9L	0.1417	0.0379
D_{in}_13R										13R←47L	0.1178	0.0153
E_{loc}_32L										32L←7L	0.1417	0.0153

Second, meta research showed that the ventrolateral prefrontal cortex (VLPFC) is often activated in the process of various lying tasks [47]. Abe et al., indicated that the VLPFC is engaged in the process of inhibiting honest answers [48]. These studies demonstrated its function of inhibitory control in working memory. The MIIFs in our study include two connectivity within the VLPFC: between BA 10L and BA 44R on alpha and beta bands. Based on previous findings, these two flows may suggest that the subjects in the guilty group inhibit the truthful response and hence altering the truthful response, which could be partly consistent with reports that the alpha desynchronization is generally related to the difficulty of a task and also the increased demands for attention or cognitive load or motor control. In sum, we speculated that the information flows within the VLPFC might reflect how guilty subjects put more attention and cognitive skills in completing a more difficult task. Specifically, the guilty subjects made additional efforts needed to "overcome" the inhibited true response, compared with the innocent subjects

Third, we can see from Fig. 7 that there are two MIIFs between VLPFC and DLPFC (from BA 46R to BA 44R on theta band and from BA 10L to BA 9L on beta band). Combined with the previous findings regarding the functional significance of theta rhythm synchronization between two cortices [49]-[54], we hypothesized that the MIIF from BA 46R to BA 44R might represent the brain activity of the episodic memory and new information encoding. In addition, although current related studies about the functional significance of the beta band suggest that its oscillation is associated with visual perceptual decision-making [55], considering the above discussed brain function of BA 10 and BA 9, we speculated that the information flow from BA 10L to BA 9L shows that the guilty subjects were required to inhibit not only the truthful response but also the truthful memory, which is worthy of future research.

Fourth, although many studies have demonstrated the synchronization activation of the premotor cortex (BA6) and frontal cortex when deceptive behaviors occurred [56], [57], whether and how these brain regions communicated has not yet been deeply investigated. In our study, the influence of BA 46R to BA 6L on delta, alpha and beta bands further

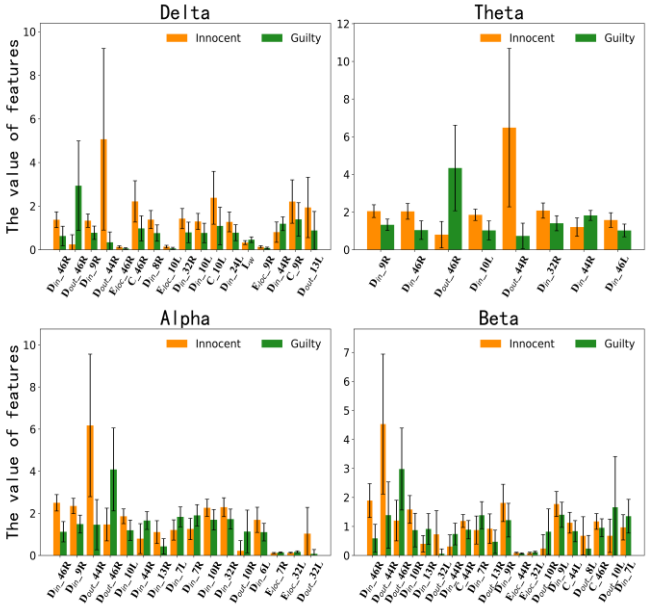

Fig. 6. Comparisons in the feature values between the two groups. All the comparisons yielded significant differences as determined by the independent sample t-test, two tailed. Error bar denotes SD of the mean. The values are given in the form of the mean ± SD. The local features of ROI are given in the form of the name of the measure _the name of BA (L: left; R: right).

demonstrated that during deception, there is communication between the premotor cortex and frontal cortex, and we speculate that, this result might reflect how the frontal cortex gives an instruction or command to the premotor cortex to complete specific tasks related to response inhibition and selection.

Regarding the information flow between the frontal and parietal cortices, we found a total of 4 MIIFs, in which the precuneus (BA 7) played a prominent role. The contextual system, however, mainly involved the prefrontal cortex. In contrast, the attentional system includes the parietal and insular cortex and subcortical nuclei. First, Langleben et al., reported the synchronization and activation of the frontal and parietal cortices in a lie detection study and showed that the attentional orientation system is always involved in the visual target and

novelty processing, while the working memory system is involved in contextual processing [1]. Furthermore, humans have two separable and parallel control networks, i.e., frontal-parietal and cingulo-opercular networks [58]-[60]. Previous studies have reported that completion of various tasks, including episodic memory, retrieval and self-processing operations require the involvement of the precuneus [61]. Since various tasks are inseparable from participation in this brain area combined with the function roles of the frontal cortex (DLPFC and VLPFC) reported in most previous lying studies, we speculated that the information flows including BA 46R to 7L and BA 7L to BA 44R indicate a completed episodic memory retrieval circuit (communication between the brain areas of episodic and working memory), which suggests more load of the memory-related and executive control processes when guilty subjects faced P stimuli in contrast to the innocent subjects. Some lie detection studies have suggested that frontoparietal activation may reflect executive functioning [62]. Some researchers also found the activation of the frontal-parietal network in the delta band [63] and proposed that it is involved in top-down processes during task-switching [64], [65]; others argued that it represents the higher cognitive and executive response load in guilty subjects [58]. For the information flow on alpha and beta, previous studies have shown that alpha oscillations are consistently implicated during task switching [66] and experimental results indicated stronger desynchronization in alpha and beta activity within brain areas of the fronto-parietal network when a switch in task was performed. Hence, three information flows from BA 46 and BA 10 to BA 7 on the alpha/beta band, and from BA 47L

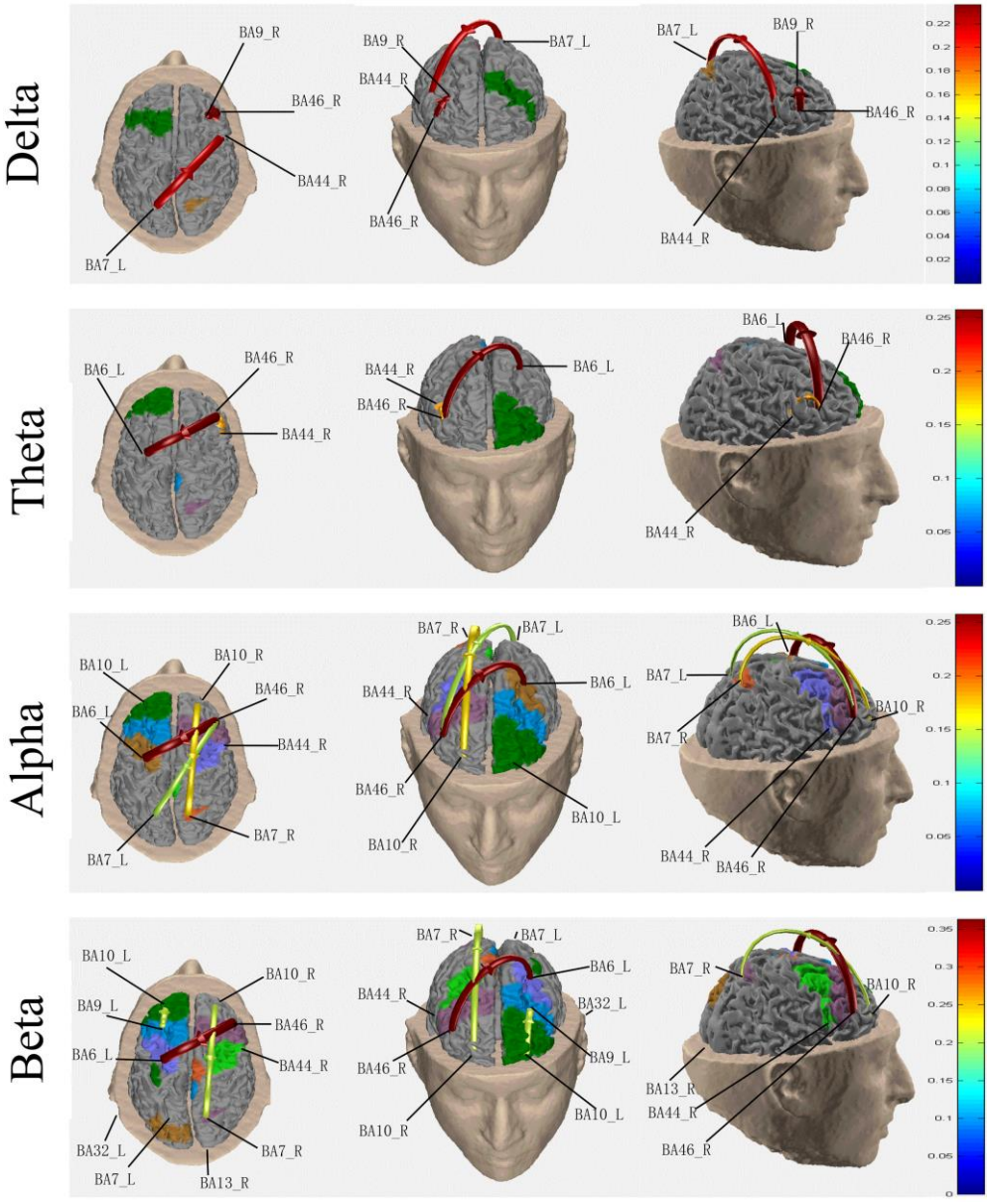

Fig. 7. The MIIFs for each band. Each ROI is represented in a different color. There are 2, 2, 4, 7 MIIFs for delta, theta, alpha and beta bands, respectively (also see Table Ⅲ), and they are represented with arrows that move from a cortical area (source) toward another one (target). The flows' color and thick code the difference of EC group mean between the two groups. The 3-D EC network is drawn using the eConnectome toolbox ([40]).

(VLPFC) to BA 13R (insular) on the beta band demonstrate not only the cooperation of the attentional system and contextual processing system in higher bands, but also the stronger frontal-parietal network's involvement in task switching during the lying behavior, compared to the innocent behaviors.

2) ACC and its MIIFs

Among the MIIFs, there is a flow from BA 7L to BA 32L (Dorsal anterior cingulate cortex, ACC). First, many fMRI-based deception investigations have reported increased activation in the ACC, and distinguished this region from DLPFC in functional roles in the process of lying and suggested its function of monitoring stronger cognitive conflict [41], [48], [67]-[71]. Furthermore, most studies have demonstrated that the beta oscillations were associated with visual perceptual decision-making [55]. Considering the episodic memory function of the precuneus (BA 7) during deceptive tasks, one reasonable inference for the finding of this beta MIIF is that after guilty subjects saw the stolen objects, the precuneus cortex was activated by the episodic memory function, and subsequently, stronger conflict occurred which was monitored by the ACC. Overall, when a guilty subject saw a stolen object, a more complex or difficult recognition and also a stronger conflict monitor was elicited, compared with the truth-telling tasks.

B. Classification of the deception response

It is worthy pointing out the importance of the feature selection of the two steps. Especially since we emphasize that based on those features with significant differences between the two groups, which were selected in the first step, we combined a classification strategy with F_score algorithm to select the final features, aimed at achieving high classification performance. The classification result shows that truth-telling could be differentiated from lying with a high *BTA* of 99.06%, taking the beta band as an example (see Table II). According to our viewpoint, only the features with high classification performance could represent the important difference in neural activity between truth-telling and lie-telling.

C. Network parameters based on graph theory

Graph theory can extract local and global features in connectivity patterns. Using this approach, we finally proposed several focused measures to construct an optimal classifier for each frequency band. These proposed measures imply more extra workload in specific brain regions during lying, relative to truth telling. Among these measures, we can clearly find some important “hub” in the effective connectivity network, including BA 7, BA 44, BA 46, and so on. In fact, the MIIFs were derived from these crucial brain regions. In sum, for the study of deception the implication of the graph theory was critical in exploring the important information flows between critical cortices. From the optimal feature subset, we only focused on and selected the measures whose values were significantly greater in the guilty group than in the innocent group. Due to limited space, we neglected the other measures in this study. Thus, whether those neglected measures hide valuable information on the brain mechanism of deception remains to be explored in a future study.

D. Limitations

Although our findings are novel, some limitations are worth considering. Firstly, EEG signals from 64 channels were recorded. However, theoretically, only enough recording electrodes could obtain an accurate location of all cortex sources. Insufficient electrodes could affect the accuracy of source location. In addition, we selected the ROI based on most of the previous lie detection studies. For example, the difference in the experimental protocol between the present and the studies may have resulted in the difference in brain activity. Furthermore, we have not source located neural activity on the non-cortex. However, some researchers found the involvement of thalamic nuclei [41] or caudate nucleus during deception [72], [73]. The above named factors would result in insufficient investigation into the neural process, brain cooperation between different brain regions and the biological mechanisms of deception.

Secondly, our protocol designs probably could not sufficiently cover possible real-life instructed lying scenarios. To address this issue, we tried to imitate crime scene true stories of crime and detection. In spite of this effort, some emotional components (e.g., fear and anxiety that should be the essential components in the deception from real life) could not be covered by the condition of the mock crime. Currently, some researchers have argued as to whether the protocol in LD studies should include as many emotional elements as possible. In addition, we did not investigate the effect of the countermeasure on the lie detection. Some researchers have demonstrated that simple countermeasures could affect the GKT [56]. A future study could, therefore, improve the GKT protocol using a new design to resist a countermeasure.

Furthermore, PDC method was employed to analyze effective connectivity in four different frequency bands. Accordingly, the MIIFs obtained here were presented in four bands. Although our interpretation of most of the MIIFs is basically consistent with current research findings, there is still difficulty in interpreting some information flows. For example, why does the connectivity between BA 10L and BA 44R occur in the beta band? It is commonly accepted that there are different brain functions for different EEG oscillations. Unfortunately, there is no extensive research that has been conducted on the specific brain function of each EEG oscillation. Thus, combining our understanding of the neurophysiology of different EEG frequency bands with the findings of EEG information flows to explore the neural mechanism of the deception deserves deep investigation.

Finally, a growing number of studies on neuroscience have reported great advantages of fusion features. For example, Sun et al. suggested that combining the recording of the EEG and fMRI could provide more complete and richer information from spatial and temporal variation features [74]. Hence, one of the future research goals is to employ multimodal fusion approaches to provide more spatiotemporal information of the neural process during deception and hence enhance the accuracy of LD.

Ⅴ. CONCLUSION

In the present study, we aimed to analyze cortical effective

connectivity in order to detect deception by adopting partial directed coherence on cortical potentials estimated from multi-channel EEG. First, our results indicate that between lying and telling the truth there is a significant difference in the brain communication and cooperation mode reflected by the proposed and most important information flows between different brain cortices. Based on the experimental result obtained from the application of graph theory tools to the functional connectivity networks, we distinguished the liars from the innocent subjects using the SVM-based classification mode. The results strongly support the view that it is reasonable and feasible to utilize the PDC method in source space to detect deceptive responses and hence to differentiate guilty subjects from innocent subjects. Furthermore, some important communications especially between the frontal cortex and the parietal cortex are involved in and supported the lying behaviors. Particularly, based on the findings of the MIIFs, we found evidence that three systems are involved in brain cognitive activity of deception behaviors. Specifically, the attention system represented by the parietal cortex, the contextual system represented by the frontal cortex and the conflict monitoring system represented by the ACC cooperated to complete working memory updating, episodic memory retrieval, task switching and response inhibition. The connectivity related to the frontal-parietal networks are most discriminating, implying crucial roles for this network in the processing of deception. In contrast to most previous LD studies, this investigation provides a new research method for LD and the present findings broaden our understanding of the brain cooperative mechanism underlying deception.

Ⅶ. Conflict of interest

The authors have declared that no competing interests exist.

Ⅷ. Funding

This work was supported by the National Nature Science Foundation of China (grant No. 61773408, 81271659, 62071177, 61872405, 81571049 and 81870863)

Ⅸ. Acknowledgements

The authors wish to greatly thank Li Feng for programing and collecting data, Shao Shi-Yun for suggesting the revision work of this paper.

References

[1]D. D. Langleben, *et al.*, "Telling truth from lie in individual subjects with fast event-related fMRI," *Hum. Brain Mapp.,* vol. 26, no. 4, pp. 262-272, Dec 2005.

[2]Q. Cui, *et al.*, "Detection of deception based on fMRI activation patterns underlying the production of a deceptive response and receiving feedback about the success of the deception after a mock murder crime," *Soc. Cogn. Affect. Neurosci.,* vol. 9, no. 10, pp. 1472-1480, Oct 2014.

[3]C. Davatzikos, *et al.*, "Classifying spatial patterns of brain activity with machine learning methods: application to lie detection," *NeuroImage,* vol. 28, no. 3, pp. 663-668, Nov 2005.

[4]V. Abootalebi, M. H. Moradi, and M. A. Khalilzadeh, "A new approach for EEG feature extraction in P300-based lie detection," *Comput. Methods Programs Biomed.,* vol. 94, no. 1, pp. 48-57, Apr 2009.

[5]E. H. Meijer, *et al.*, "The P300 is sensitive to concealed face recognition," *Int. J. Psychophysiol.,* vol. 66, no. 3, pp. 231-237, 2007.

[6]L. A. Farwell, D. C. Richardson, and G. M. Richardson, "Brain fingerprinting field studies comparing P300-MERMER and P300 brainwave responses in the detection of concealed information," *Cogn. Neurodyn.,* vol. 7, no. 4, pp. 263-299, Aug 2013.

[7]X. Deng, *et al.*, "Superiority of visual (verbal) vs. auditory test presentation modality in a P300-based CIT: The Complex Trial Protocol for concealed autobiographical memory detection," *Int. J. Psychophysiol.,* vol. 105, pp. 26-34, Jul 2016.

[8]J. Gao, *et al.*, "A novel concealed information test method based on independent component analysis and support vector machine," *Clin. EEG Neurosci.,* vol. 43, no. 1, pp. 54-63, Jan 2012.

[9]J. Gao, *et al.*, "A novel algorithm to enhance P300 in single trials: Application to lie detection using F-score and SVM," *PLoS One,* vol. 9, no. 11, p. e109700, 2014.

[10]J. Gao, *et al.*, "A novel approach for lie detection based on F-score and extreme learning machine," *PLoS One,* vol. 8, no. 6, p. e64704, 2014.

[11]J. Gao, *et al.*, "Denoised P300 and machine learning-based concealed information test method," *Comput. Methods Programs Biomed.,* vol. 104, no. 3, pp. 410-417, Dec 2011.

[12]F. Varela, *et al.*, "The brainweb: phase synchronization and large-scale integration," *Nat. Rev. Neurosci.,* vol. 2, no. 4, pp. 229-239, Apr 2001.

[13]G. Ganis, *et al.*, "Neural correlates of different types of deception: an fMRI investigation," *Cereb. Cortex,* vol. 13, no. 8, pp. 830-836, Aug 2003.

[14]A. A. Karim, *et al.*, "The truth about lying: inhibition of the anterior prefrontal cortex improves deceptive behavior," *Cereb. Cortex,* vol. 20, no. 1, pp. 205-213, 2010.

[15]J. F. Gao, *et al.*, "Exploring time- and frequency- dependent functional connectivity and brain networks during deception with single-trial event-related potentials," *Sci. Rep.,* vol. 6, p. 37065, Nov 2016.

[16]H. Wang, W. Chang, and C. Zhang, "Functional brain network and multichannel analysis for the P300-based brain computer interface system of lying detection," *Expert Syst. Appl.,* vol. 53, pp. 117-128, 2016.

[17]Y. Wang, *et al.*, "An electroencephalography network and connectivity analysis for deception in instructed lying tasks," *PLoS One,* vol. 10, no. 2, p. e0116522, 2015.

[18]F. D. V. Fallani, *et al.*, "Cortical functional connectivity networks in normal and spinal cord injured patients: Evaluation by graph analysis," *Hum. Brain Mapp.,* vol. 28, no. 12, pp. 1334-1346, Dec 2007.

[19]F. Babiloni, *et al.*, "Estimation of the cortical functional connectivity with the multimodal integration of high-resolution EEG and fMRI data by directed transfer function," *NeuroImage,* vol. 24, no. 1, pp. 118-131, Jan 2005.

[20]V. Sakkalis, "Review of advanced techniques for the estimation of brain connectivity measured with EEG/MEG," *Comput. Biol. Med.,* vol. 41, no. 12, pp. 1110-1117, Dec 2011.

[21]L. Astolfi, *et al.*, "Tracking the time-varying cortical connectivity patterns by adaptive multivariate estimators," *IEEE Trans. Biomed. Eng.,* vol. 55, no. 3, pp. 902-913, Mar 2008.

[22]L. Astolfi, *et al.*, "Assessing cortical functional connectivity by partial directed coherence: simulations and application to real data," *IEEE Trans. Biomed. Eng.,* vol. 53, no. 9, pp. 1802-1812, Sep 2006.

[23]G. Pfurtscheller and F. H. Lopes da Silva, "Event-related EEG/MEG synchronization and desynchronization: basic principles," *Clin. Neurophysiol.,* vol. 110, no. 11, pp. 1842-1857, Nov 1999.

[24]S. P. van den Broek, *et al.*, "Volume conduction effects in EEG and MEG," *Electroencephalogr. Clin. Neurophysiol.,* vol. 106, no. 6, pp. 522-534, Jun 1998.

[25]C. Phillips, M. D. Rugg, and K. J. Fristont, "Systematic regularization of linear inverse solutions of the EEG source localization problem," *NeuroImage,* vol. 17, no. 1, pp. 287-301, Sep 2002.

[26]A. Delorme and S. Makeig, "EEGLAB: an open source toolbox for analysis of single-trial EEG dynamics including independent component analysis," *J. Neurosci. Methods,* vol. 134, no. 1, pp. 9-21, Mar 2004.

[27]R. D. Pascual-Marqui, "Standardized low-resolution brain electromagnetic tomography (sLORETA): technical details," *Methods Find. Exp. Clin. Pharmacol.,* vol. 24 Suppl D, pp. 5-12, 2002.

[28]K. J. Blinowska, R. Kus, and M. Kaminski, "Granger causality and information flow in multivariate processes," *Phys. Rev. E: Stat., Nonlinear, Soft Matter Phys.,* vol. 70, no. 5, p. 050902, Nov 2004.

[29]E. Bullmore and O. Sporns, "Complex brain networks: graph theoretical analysis of structural and functional systems," *Nat. Rev. Neurosci.,* vol. 10, no. 3, pp. 186-198, Mar 2009.

[30]M. Rubinov and O. Sporns, "Complex network measures of brain

connectivity: uses and interpretations," *NeuroImage,* vol. 52, no. 3, pp. 1059-1069, Sep 2010.

[31]C. J. Stam*, et al.*, "Small-world networks and functional connectivity in Alzheimer's disease," *Cereb. Cortex,* vol. 17, no. 1, pp. 92-99, Jan 2007.

[32]M. Rubinov*, et al.*, "Brain connectivity toolbox: a collection of complex network measurements and brain connectivity datasets," *NeuroImage,* no. 47, p. S169, 2009.

[33]N. Nnamoko et al., "Evaluation of filter and wrapper methods for feature selection in supervised machine learning," in *Proc. 15th Annu. Postgraduate Symp. Convergence Telecommunication, Netw. Broadcast.*, 2014.

[34]D. A. Peterson*, et al.*, "Feature selection and blind source separation in an EEG-based brain-computer interface," *EURASIP J. Adv. Signal Process.,* vol. 2005, no. 19, pp. 1-13, 2005.

[35]J. Gao*, et al.*, "Brain Fingerprinting and Lie Detection: A Study of Dynamic Functional Connectivity Patterns of Deception Using EEG Phase Synchrony Analysis," *IEEE J. BIOMED. HEALTH.,* 2021.

[36]S. Y. Shao*, et al.*, "Automatic EEG artifact removal: a weighted support vector machine approach with error correction," *IEEE Trans. Biomed. Eng.,* vol. 56, no. 2, pp. 336-344, Feb 2009.

[37]K. Polat and S. Güneş, "A new feature selection method on classification of medical datasets: Kernel F-score feature selection," *Expert Syst. Appl.,* vol. 36, no. 7, pp. 10367-10373, 2009.

[38]P. Li*, et al.*, "EEG Based Emotion Recognition by Combining Functional Connectivity Network and Local Activations," *IEEE Trans. Biomed. Eng.,* vol. 66, no. 10, pp. 2869-2881, Oct 2019.

[39]F. L. Chen and F. C. Li, "Combination of feature selection approaches with SVM in credit scoring," *Expert Syst. Appl.,* vol. 37, no. 7, pp. 4902-4909, 2010.

[40]B. He*, et al.*, "eConnectome: A MATLAB toolbox for mapping and imaging of brain functional connectivity," *J. Neurosci. Methods,* vol. 195, no. 2, pp. 261-269, Feb 2011.

[41]J. M. Nunez*, et al.*, "Intentional false responding shares neural substrates with response conflict and cognitive control," *NeuroImage,* vol. 25, no. 1, pp. 267-277, Mar 2005.

[42]H. C. Leung, J. C. Gore, and P. S. Goldman-Rakic, "Sustained mnemonic response in the human middle frontal gyrus during on-line storage of spatial memoranda," *J. Cogn. Neurosci.,* vol. 14, no. 4, pp. 659-671, May 15 2002.

[43]J. R. Pedersen*, et al.*, "Origin of human motor readiness field linked to left middle frontal gyrus by MEG and PET," *NeuroImage,* vol. 8, no. 2, pp. 214-220, Aug 1998.

[44]A. Priori*, et al.*, "Lie-specific involvement of dorsolateral prefrontal cortex in deception," *Cereb. Cortex,* vol. 18, no. 2, pp. 451-455, Feb 2008.

[45]K. Sakai, J. B. Rowe, and R. E. Passingham, "Active maintenance in prefrontal area 46 creates distractor-resistant memory," *Nat. Neurosci.,* vol. 5, no. 5, pp. 479-484, May 2002.

[46]R. Ishii*, et al.*, "Cortical oscillatory power changes during auditory oddball task revealed by spatially filtered magnetoencephalography," *Clin. Neurophysiol.,* vol. 120, no. 3, pp. 497-504, Mar 2009.

[47]S. E. Christ*, et al.*, "The contributions of prefrontal cortex and executive control to deception: evidence from activation likelihood estimate meta-analyses," *Cereb. Cortex,* vol. 19, no. 7, pp. 1557-1566, Jul 2009.

[48]N. Abe*, et al.*, "Dissociable roles of prefrontal and anterior cingulate cortices in deception," *Cereb. Cortex,* vol. 16, no. 2, pp. 192-199, Feb 2006.

[49]W. Klimesch, "EEG alpha and theta oscillations reflect cognitive and memory performance: a review and analysis," *Brain Res Brain Res Rev,* vol. 29, no. 2-3, pp. 169-195, Apr 1999.

[50]W. Klimesch*, et al.*, "Episodic retrieval is reflected by a process specific increase in human electroencephalographic theta activity," *Neurosci. Lett.,* vol. 302, no. 1, pp. 49-52, 2001.

[51]W. Klimesch*, et al.*, "Theta synchronization during episodic retrieval: neural correlates of conscious awareness," *Brain Res Brain Res Rev,* vol. 12, no. 1, pp. 33-38, Aug 2001.

[52]S. P. Muthukrishnan, S. Soni, and R. J. B. t. Sharma, "Brain networks communicate through theta oscillations to encode high load in a visuospatial working memory task: an EEG connectivity study," *Brain Topogr.,* vol. 33, no. 1, pp. 75-85, 2020.

[53]P. Sauseng, W. J. N. Klimesch, and B. Reviews, "What does phase information of oscillatory brain activity tell us about cognitive processes?" *Neurosci. Biobehav. Rev.,* vol. 32, no. 5, pp. 1001-1013, 2008.

[54]B. Tóth*, et al.*, "EEG synchronization characteristics of functional connectivity and complex network properties of memory maintenance in the delta and theta frequency bands," *Int. J. Psychophysiol.,* vol. 83, no. 3, pp. 399-402, Mar 2012.

[55]G. B. Chand, B. Lamichhane, and M. Dhamala, "Face or House Image Perception: Beta and Gamma Bands of Oscillations in Brain Networks Carry Out Decision-Making," *Brain Connect,* vol. 6, no. 8, pp. 621-631, Oct 2016.

[56]G. Ganis*, et al.*, "Lying in the scanner: covert countermeasures disrupt deception detection by functional magnetic resonance imaging," *NeuroImage,* vol. 55, no. 1, pp. 312-319, Mar 2011.

[57]D. D. Langleben*, et al.*, "Brain activity during simulated deception: an event-related functional magnetic resonance study," *NeuroImage,* vol. 15, no. 3, pp. 727-732, Mar 2002.

[58]N. U. Dosenbach*, et al.*, "A dual-networks architecture of top-down control," *Trends Cognit. Sci.,* vol. 12, no. 3, pp. 99-105, Mar 2008.

[59]N. U. Dosenbach*, et al.*, "Prediction of individual brain maturity using fMRI," *Science,* vol. 329, no. 5997, pp. 1358-1361, 2010.

[60]W. Jiang*, et al.*, "Decoding the processing of lying using functional connectivity MRI," *Behav. Brain Funct.,* vol. 11, no. 1, pp. 1-11, 2015.

[61]A. E. Cavanna and M. R. Trimble, "The precuneus: a review of its functional anatomy and behavioural correlates," *Brain,* vol. 129, no. Pt 3, pp. 564-583, Mar 2006.

[62]E. K. Jung, K. Y. Kang, and Y. Y. Kim, "Frontoparietal activity during deceptive responses in the P300-based guilty knowledge test: an sLORETA study," *NeuroImage,* vol. 78, pp. 305-315, Sep 2013.

[63]M. E. López*, et al.*, "Dynamic low frequency EEG phase synchronization patterns during proactive control of task switching," *NeuroImage,* vol. 186, pp. 70-82, Feb 2019.

[64]L. Cocchi*, et al.*, "Dynamic cooperation and competition between brain systems during cognitive control," *Trends Cognit. Sci.,* vol. 17, no. 10, pp. 493-501, 2013.

[65]E. L. Mansfield, F. Karayanidis, and M. X. Cohen, "Switch-related and general preparation processes in task-switching: evidence from multivariate pattern classification of EEG data," *J. Neurosci.,* vol. 32, no. 50, pp. 18253-18258, Dec 2012.

[66]A. L. Proskovec, A. I. Wiesman, and T. W. Wilson, "The strength of alpha and gamma oscillations predicts behavioral switch costs," *NeuroImage,* vol. 188, pp. 274-281, Mar 2019.

[67]C. S. Carter*, et al.*, "Anterior cingulate cortex, error detection, and the online monitoring of performance," *Science,* vol. 280, no. 5364, pp. 747-749, May 1998.

[68]J. C. Dreher and K. F. Berman, "Fractionating the neural substrate of cognitive control processes," *Proc. Natl. Acad. Sci. U. S. A.,* vol. 99, no. 22, pp. 14595-14600, Oct 2002.

[69]H. Garavan*, et al.*, "Dissociable executive functions in the dynamic control of behavior: inhibition, error detection, and correction," *NeuroImage,* vol. 17, no. 4, pp. 1820-1829, Dec 2002.

[70]J. G. Kerns*, et al.*, "Anterior cingulate conflict monitoring and adjustments in control," *Science,* vol. 303, no. 5660, pp. 1023-1026, Feb 2004.

[71]A. W. MacDonald*, et al.*, "Dissociating the role of the dorsolateral prefrontal and anterior cingulate cortex in cognitive control," *Science,* vol. 288, no. 5472, pp. 1835-1838, Jun 2000.

[72]M. Kireev*, et al.*, "Functional interactions between the caudate nuclei and inferior frontal gyrus providing deliberate deception," *Hum. Physiol.,* vol. 41, no. 1, pp. 22-26, 2015.

[73]M. Kireev*, et al.*, "Deception related changes in functional connectivity between prefrontal cortex and caudate nucleus," *Int. J. Psychophysiol.,* vol. 2, no. 94, p. 123, 2014.

D. Sun, T. M. Lee, and C. C. H. Chan, "Unfolding the spatial and temporal neural processing of lying about face familiarity," *Cereb. Cortex,* vol. 25, no. 4, pp. 927-936, 2015

[74] D. D. Langleben, et al., "Telling truth from lie in individual subjects with fast event-related fMRI," Hum. Brain Mapp., vol. 26, no. 4, pp. 262-272, Dec 2005.